EPJ Photovoltaics **13**, 15 (2022)

https://doi.org/10.1051/epjpv/2022012

Available online at:
www.epj-pv.org

REGULAR ARTICLE OPEN ACCESS

Fluorination and chlorination effects on the charge transport properties of the IDIC non-fullerene acceptor: an ab-initio investigation★

Maria Andrea, Konstantinos Kordos, Elefterios Lidorikis, and Dimitrios Papageorgiou*

Department of Materials Science and Engineering, University of Ioannina, POB 1186, 45110 Ioannina, Greece

Received: 15 October 2021 / Received in final form: 5 April 2022 / Accepted: 20 April 2022

Abstract. Fused-ring electron acceptors end-capped with electron withdrawing groups have contributed to the ever-increasing power conversion efficiency of organic solar cells. Adding π-extensions and halogenating the end groups are two popular strategies to boost performance even further. In this work, a typical non-fullerene acceptor molecule, IDIC, is used as a model system for investigating the impact of the halogenation approach at the molecular level. The two end groups are substituted by fluorinated and chlorinated counterparts and their electronic and optical properties are systematically probed using ab-initio calculations. In gas phase, halogenation lowers the HOMO and LUMO energy levels and narrows the energy gap, especially for the chlorinated compound. Moreover, chlorinated IDIC exhibits the largest redshift and the smallest reorganization energy. Finally, crystal structures of the three compounds are constructed, revealing an improved transfer integral and transfer rate for the halogenated variants. Specifically, the chlorination strategy leads to an increase of 60% in transfer rate, compared to halogen-free IDIC.

Keywords: Organic photovoltaics / non-fullerene acceptors / IDIC / halogenation / charge transport

1 Introduction

Organic solar cells (OSCs) have been extensively investigated by the scientific community due to some of their remarkable features. They are lightweight, flexible, and can be manufactured using roll to roll printing. In the bulk heterojunction (BHJ) architecture, the active layer is based on a blend of electron donor (D) and electron acceptor (A) materials [1,2]. π-Conjugated polymers are typical donor materials while the most investigated acceptors in BHJ OSCs are fullerene-based molecules, especially $PC_{61}BM$ and $PC_{71}BM$ [3,4]. Intensive research on fullerene based BHJ solar cells has achieved power conversion efficiencies (PCEs) that exceed 10% [5,6]. Nevertheless, fullerene-based acceptors show significant drawbacks that affect the performance of OSC devices. Some of these drawbacks include weak absorption in the visible and near-infrared part of the spectrum, lack of electron level tunability and complicated synthetic routes.

Non-fullerene acceptors (NFAs) alleviate some of these difficulties. They exhibit strong absorption in the visible and near infrared spectral regions, their electronic energy levels can be tuned by chemical modifications, while their morphology can be easily manipulated. Despite their long history, they have only recently been able to demonstrate a significant increase in power conversion efficiency. A record-braking PCE of 18.07% [7] has been achieved using fused-ring electron acceptors (FREAs) [8]. FREAs are based in the A-D-A molecular design, where an electron donor core, consisting of several aromatic fused rings, combines with two electron withdrawing end groups serving as acceptors, while molecular stacking and solubility are controlled by alkyl-based side chains. The most successful end group is 1,1-dicyanomethylene-3-indanone (IC) [9] with more than 50 derivatives, being a key component to numerous NFAs such as the popular ITIC [10], IDIC [11] and Y5 [12].

Recent studies on IC-based NFAs, show that tuning the optoelectronic properties by end group modification can lead to increased performance. Such end group modifications include halogenation, π-extensions, or a combination of both [13–15]. Specifically, Li et al. [13] demonstrated that combining π-extensions and fluorination strategies in the Y5 NFA can lead up to a PCE of 16.6%. π-Extensions increase electronic delocalization leading to a redshift in

★ This paper is based on the contribution (and published after the peer-review and acceptation) at the 'ISFOE21:14th International Symposium on Flexible Organic Electronics, Nanotexnology Event 2021'.

* e-mail: dpapageo@uoi.gr

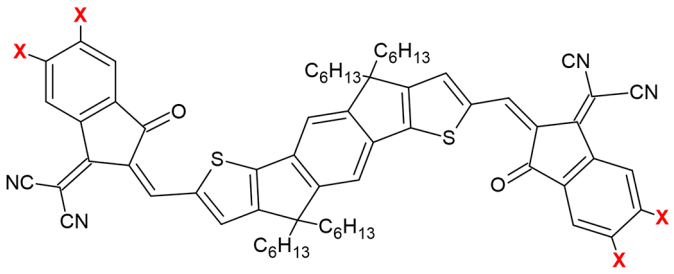

Fig. 1. Chemical structure of the IDIC non-fullerene acceptor (X = H). Halogenated variants are obtained by substituting X with F or Cl.

the optical absorption spectrum. However, halogenation also provides an effective way to tune the optoelectronic properties of NFAs. Specifically, halogenation (including chlorination and fluorination) is used to adjust the highest occupied molecular orbital (HOMO) and the lowest unoccupied molecular orbital (LUMO) in order to achieve a proper donor-acceptor energy offset [16,17]. Fluorination lowers the HOMO and LUMO energy levels and improves intermolecular interaction that is crucial for enhanced electron mobility [13,18–20]. Moreover, several studies have shown that chlorination is more effective in decreasing LUMO energy level leading to a stronger π-stacking and finally to increased exciton delocalization [21–23]. Computational studies proposing new NFA designs aiming at performance enhancement are also available in the literature. These include asymmetric modifications of the Y6 acceptor [24], introduction of new fused ring units in ITIC end groups [25], replacement of the toxic cyano moiety [26] in the IC end groups, 2D and quad-rotor shaped novel NFAs [27,28].

Here, we focus on a representative fused-ring NFA molecule, IDIC, namely 2,2′-((2Z,2′Z)-((4,4,9,9-tetrahexyl-4,9-dihydro-s-indaceno[1,2-b:5,6-b′]dithiophene-2,7-diyl) bis(methanylylidene))bis(3-oxo-2,3-dihydro-1H-indene-2,1-diylidene))dimalononitrile. This molecule consists of a fully fused indacenodithiophene (IDT) core, two 1,1-dicyano-methylene-3-indanone electron withdrawing units and four n-hexyl side chains (Fig. 1) [11,29,30]. IDIC can be easily synthesized and PCE exceeds 13% when combined with the PTQ10 polymeric donor [31]. Moreover, it has been used in ternary OPVs [32] as well as in planar perovskite solar cells as a replacement of TiO_2 in the electron transport layer [33].

In this work we investigate the effects of chlorination and fluorination in the IC end groups, taking IDIC as a model system. The chemical structure of pristine IDIC (IDIC-4H) along with its chlorine (IDIC-4Cl) and fluorine (IDIC-4F) substituted counterparts is shown in Figure 1. For all three compounds we compare frontier molecular orbital (FMO) distributions, reorganization energies, electron affinities and ionization potentials as well as the total and partial density of states calculated in gas phase with DFT methods. The absorption spectra of the three species are also studied using TD-DFT. Finally, the experimental crystal structure is used as a reference and the values of electron transfer integrals and transfer rates are estimated.

2 Computational methods

2.1 DFT computations

DFT was employed for all structural relaxations and single point computations. The geometries of the three different derivatives, IDIC-4H, IDIC-4F, IDIC-4Cl, were fully optimized in gas phase, in the neutral, anionic and cationic states, utilizing the hybrid B3LYP functional [34–35] along with the 6-31G(d,p) basis set. This method was chosen since it provides accurate results at low computational costs [36–38]. After each geometry optimization, the vibrational frequencies were examined in order to confirm that the stationary point found by the optimizer is a true energy minimum. B3LYP/6-31G(d,p) was also applied for extracting the frontier molecular orbital distributions in the ground state, energy gaps, as well as the total and partial density of states. Absorption spectra of the three species were derived by applying TD-B3LYP/6-31G(d,p) to the previously optimized geometries, obtaining electronic transitions up to ten states. Structural relaxations in the bulk were performed using the PBE exchange and correlation functional [39,40] along with an ultrasoft pseudopotential [41] combined with a plane wave basis, setting the energy cutoff to 39 Ry. DFT computations in the gas phase were performed with Gaussian03 [42] while the Quantum Espresso package [43,44] was employed for computations in the bulk. Absorption spectra and total and partial density of states were extracted utilizing the GaussSum software [45]. Calculations for reorganization energy, electron affinity and ionization potential were performed utilizing the B3LYP/6-31G(d,p) level of theory in the NWChem software package [46], enforcing tight scf and optimization convergence.

2.2 Electron affinity and ionization potential

Electron affinity (EA) and ionization potential (IP), both vertical and adiabatic, were calculated using the standard definitions:

$$EA^{ad} = U_{nN} - U_{aA}$$

$$EA^{v} = U_{nN} - U_{aN}$$

$$IP^{ad} = U_{cC} - U_{nN}$$

$$IP^{v} = U_{cN} - U_{nN}$$

where U_{nN}, U_{aA} denote the total energy of the neutral and anionic states, while U_{aN} is the total energy of the anion in the geometry of the neutral state. Furthermore, U_{cC}, U_{cN} are the total energy of the cation in the geometry of its cationic and neutral states, respectively. We note that IP and EA are used to define the fundamental gap which in turn may be approximated by the HOMO, LUMO energy levels.

2.3 Electron transfer rates

Electron hopping rate from molecule i to molecule j is described by the semi classical Marcus expression at the high temperature limit [47,48]

$$k_{ij} = \frac{J_{ij}^2}{\hbar}\sqrt{\frac{\pi}{\lambda k_B T}}\exp\left[-\frac{(\Delta G_{ij}+\lambda)^2}{4\lambda k_B T}\right]$$

where $\hbar$ is the reduced Planck's constant, k_B is the Boltzmann's constant and T is the absolute temperature. This expression captures the main parameters that affect charge transport and is widely applied to organic semiconductors since it provides a good compromise between accuracy and efficiency. According to this expression charge transfer is characterized by three basic quantities: energy difference ΔG_{ij} between initial and final states, including effects from charge polarization or an externally applied electric field, transfer integral, and reorganization energy λ. The latter is a sum of the internal and external contributions, i.e. $\lambda = \lambda_{int} + \lambda_{ext}$. The external contribution is a consequence of the rearrangement and polarization of the molecules outside the charge transfer complex and usually is considered as a constant value [49] or completely omitted, as a first approximation [50]. For efficient charge transport, λ should be small, accompanied by a sufficiently large transfer integral. In this work only the internal reorganization energy is considered.

2.4 Reorganization energy

The internal contribution to reorganization energy λ_{int} results from the rearrangement of nuclear coordinates of the two molecules composing the charge transfer complex and is computed from four points on the potential energy surface [51]. Specifically, upon electron transfer, one molecule will instantaneously become a neutral molecule, frozen at its charged molecular conformation, while the other molecule will instantaneously become a charged molecule frozen at its neutral molecular conformation. The system is considered as isolated, and any effect of the environment is ignored. Hence, λ_{int} is given by:

$$\lambda_{int} = (U_{nA} - U_{nN}) + (U_{aN} - U_{aA})$$

where U_{nN}, U_{aA} and U_{aN} are defined as in the case of EA and IP (Sect 2.2), and U_{nA} is the energy of the neutral molecule in the geometry of the anion.

2.5 Transfer integral

The electronic transfer integral between two molecules, is defined as

$$J_{ij} = \langle \phi i \mid \hat{H} \mid \phi_j \rangle$$

where $\hat{H}$ is the electronic Hamiltonian of the dimer and $\phi_{i,j}$ are wavefunctions localized on molecules i and j which participate in the charge transfer process. Adopting the frozen orbital approximation, wavefunctions $\phi_{i,j}$ correspond to the frontier molecular orbitals (LUMO, in the case of electron transfer), and the full electron wavefunction is considered as a determinant of one-electron wavefunctions. For every pair of nearby molecules (M_i, M_j), three different quantum mechanical calculations are performed. The first two refer to the isolated, uncoupled molecules M_i, M_j, while the third one refers to the molecular pair. In this work we utilize the projection method where the quantum mechanical problem is solved by the semiempirical ZINDO scheme [52]. Other quantum mechanical methods have also been used in the literature [53,54]. The required orthonormality of atomic orbitals is obtained by applying Löwdin's symmetric transformation [55]. Finally, the Hamiltonian matrix is reconstructed in the basis set of the uncoupled molecules and the transfer integral is extracted from the non-diagonal elements.

Transfer integrals are highly sensitive to orientation and distance of the molecules participating in the charge transfer. Therefore, its calculation should be performed for every neighboring pair of molecules in the system. The radial distribution function (RDF) of the bulk configuration is used to define an appropriate distance cut-off in order to construct a precise list of neighboring molecules. Two molecules are considered as neighbors if the distance between the center of mass of the IDT core or the IC end groups is less or equal than the chosen cutoff. In order to speed up the procedure, computations on the pair were performed using an initial orbital guess, based on the orbitals of the two monomers [53] and the procedure was carried out applying the B3LYP/6-31G(d,p) level of theory using Gaussian03 software package [42].

3 Results and discussion

3.1 Gas phase

Gas phase geometry optimization on the parent, IDIC-4H, and the halogenated compounds, IDIC-4F and IDIC-4Cl, revealed no significant difference, yielding perfectly planar structures in all three cases. Contour plots of the FMOs are compared in Figure 2. Electron density of the HOMO orbital is strengthened over the electron-rich IDT core, while it appears considerably weakened over the two edge IC units. On the other hand, electron density of the LUMO orbital is equally spread over the IDT backbone, while density on the edge units appears to be much higher in the case of LUMO. These results are in line with the A-D-A architecture of the IDIC NFA and support the idea that the IC end units play an

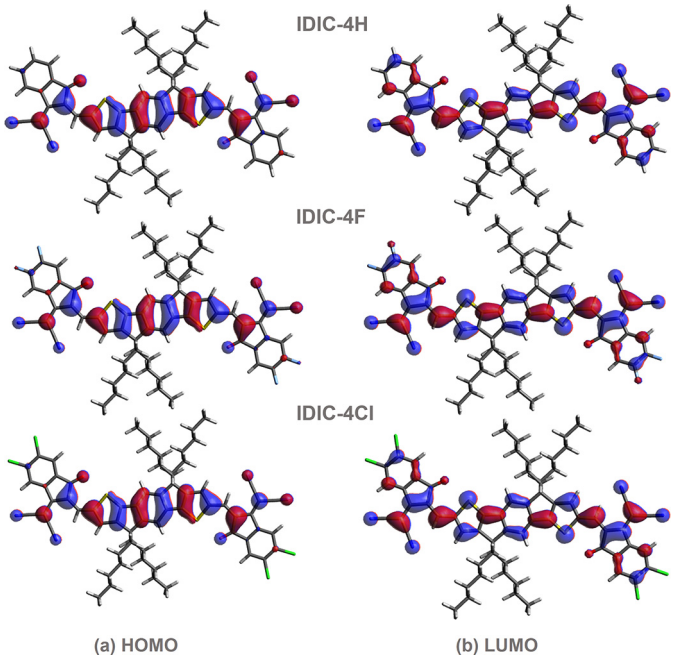

Fig. 2. Orbital distributions for the three compounds IDIC-4H, IDIC-4F, IDIC-4Cl. (a) HOMO, (b) LUMO.

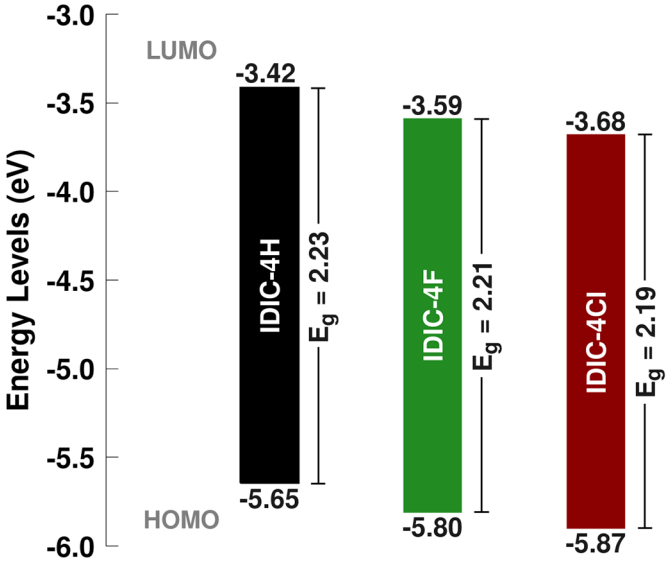

Fig. 3. HOMO, LUMO energy levels for the three compounds. The related energy gaps are also displayed.

essential role to the charge transfer mechanism. They are also in agreement with Qu et al. [21], where the same behavioral pattern is observed for tetrafluorinated ITIC [18].

Although introduction of fluorine and chlorine atoms to the IC end groups does not significantly affect HOMO and LUMO distributions, it lowers however the corresponding energy levels following the order: $LUMO_{IDIC\text{-}4H}$ (–3.42 eV) > $LUMO_{IDIC\text{-}4F}$ (–3.59 eV) > $LUMO_{IDIC\text{-}4Cl}$ (–3.68 eV) and $HOMO_{IDIC\text{-}4H}$ (–5.65 eV) > $HOMO_{IDIC\text{-}4F}$ (–5.80 eV) > $HOMO_{IDIC\text{-}4Cl}$ (–5.87 eV). It also slightly narrows the related energy gaps that range between 2.23 eV for IDIC-4H and 2.19 eV for IDIC-4Cl. Decrease in the LUMO level due to fluorination has also been reported in the literature for the Y5 [13] and ITIC [18] NFAs. Compared to fluorination, chlorination is more effective in decreasing HOMO and LUMO energy levels, due to chlorines' ability to accommodate greater electron density, even though fluorine is a more electronegative atom than chlorine. The same effect has also been observed in several small organic semiconductors such as acenes and phthalocyanines [21–23]. The results reveal that IDIC-4Cl improves the electron accepting ability and are summarized in Figure 3.

To supplement the results of the frontier molecular orbitals, total density of states (DOS) and partial density of states (PDOS) were analyzed and depicted in Figure 4. The effect of fluorination or chlorination in the DOS is minor. However, a closer look to the region around the HOMO level in the PDOS (Fig. 4d), indicates that the major contribution is related to the core IDT unit. Likewise in the region around the LUMO level, the major contribution comes from the IC end groups, in agreement with the abovementioned results for the FMO distributions.

For a deeper understanding of the influence of chlorination and fluorination on the electronic properties, we calculated the internal reorganization energies, electron affinities (EA) and ionization potentials (IP), vertical and adiabatic. The results are listed in Table 1. The smallest value of reorganization energy, among the three variants, corresponds to the chlorinated compound (0.182 eV), while the largest one corresponds to fluorinated IDIC (0.194 eV) giving a first impression that IDIC-4F may exhibit lower electron transfer rate, compared to the parent compound, and IDIC-4Cl a higher one. Aldrich et al. [18] calculated the internal reorganization energy of tetrafluorinated ITIC as 0.158 eV, slightly higher than the one for pristine ITIC (0.155 eV) while according to Yao et al. [26] the value of reorganization energy for Y6 is equal to 0.106 eV. Similar calculations yield reorganization energies lying in the range of 0.145 eV to 0.177 eV for $PC_{61}BM$ [56–58] and 0.179 eV to 0.2 eV [56,57] for $PC_{71}BM$. To sum up, the recent NFAs, ITIC and Y6, exhibit lower reorganization energy values, compared to IDIC. Contrariwise, the reorganization energy values for PCBM are comparable to the one of IDIC.

In addition, the halogenated compounds exhibit greater EA and IP values compared to the halogen-free counterpart. Apparently, the chlorinated compound not only has the highest EA, both adiabatic (2.94 eV) and vertical (2.86 eV) but the largest adiabatic (6.63 eV) and vertical (6.71 eV) IP as well. The highest EA suggests that the molecule has an increased possibility to accept an electron while the highest IP stabilizes the hole defects. Moreover, it has been reported that affinities in a range of 2–4 eV are ideal for electron stability, while fluorinated variants of Y5 exhibit larger values of EA compared to plain Y5 [13].

Absorption spectra of the three molecules are presented in Figure 5. The results tabulated in Table 2 refer to the dominant transition, being the HOMO → LUMO transition in all three cases, with a contribution of 81%. Both halogenated acceptors exhibit red-shifted absorption. For

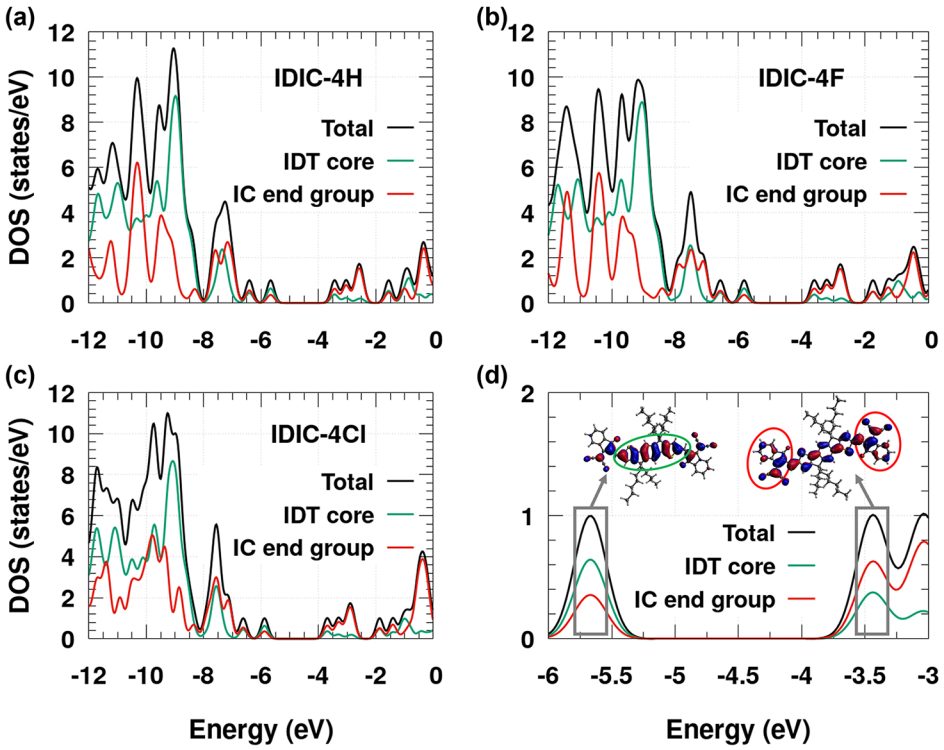

Fig. 4. Total and partial DOS for (a) the parent, (b) the fluorinated, and (c) the chlorinated compound. (d) Contributions around HOMO and LUMO energy levels for the parent molecule IDIC-4H.

Table 1. Calculated reorganization energies (λ), vertical and adiabatic electron affinities (EA) as well as ionization potentials (IP) in eV.

	λ	EA^{ad}	EA^{v}	IP^{ad}	IP^{v}
IDIC-4H	0.189	2.66	2.57	6.44	6.52
IDIC-4F	0.194	2.84	2.75	6.59	6.67
IDIC-4Cl	0.182	2.94	2.86	6.63	6.71

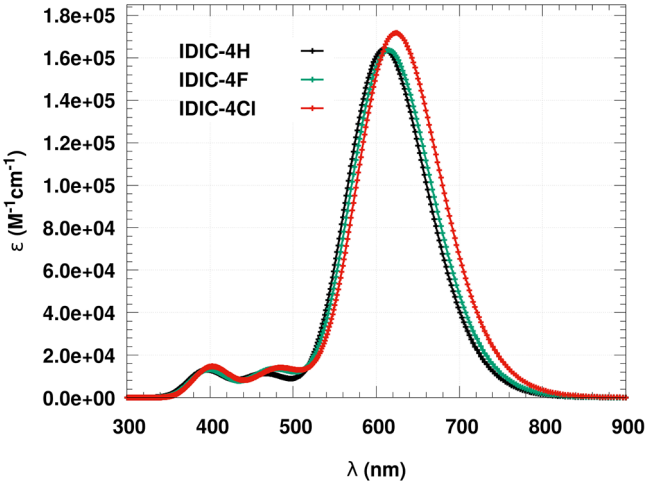

Fig. 5. Absorption spectra for the three molecules.

IDIC-4Cl, the maximum absorption is at 623 nm while for IDIC-4H at 609 nm i.e. a 14 nm redshift accompanies chlorine substitution. In case of IDIC-4F, the maximum absorption is calculated at 614 nm leading to a redshift of only 5 nm. Lastly, Qu et al. [21] determined experimentally the absorption spectrum in dilute chloroform solution of halogenated IDIC variants with a phenyl group attached to the molecular side chains. The chlorinated and fluorinated compounds exhibit an absorption maximum at 669 nm and 658 nm respectively revealing a redshift of 22 nm and 11 nm compared to pristine IDIC (647 nm). The largest calculated maximum absorption coefficient is also attributed to the chlorinated compound as well as the lowest excitation energy (1.99 eV) and the highest value of oscillator strength (2.37). The aforementioned results point out that the introduction of halogen atoms, especially chlorine atoms, in the IC end group, leads to an increased electron delocalization.

Table 2. Theoretical (λ_{max}) and experimental ($\lambda^{exp}{}_{max}$) values of maximum absorption along with the excitation energy (E_{ex}), oscillator strength (f) and transition with the major contribution.

	λ_{max} (nm)	$\lambda^{exp}{}_{max}$ (nm)[a]	E_{ex} (eV)	f	Major contribution
IDIC-4H	609	647	2.04	2.27	H→L: 81%
IDIC-4F	614	658	2.02	2.26	H→L: 81%
IDIC-4Cl	623	669	1.99	2.37	H→L: 81%

[a] Corresponds to IDIC variants with a phenyl group attached to the molecular side chains [21].

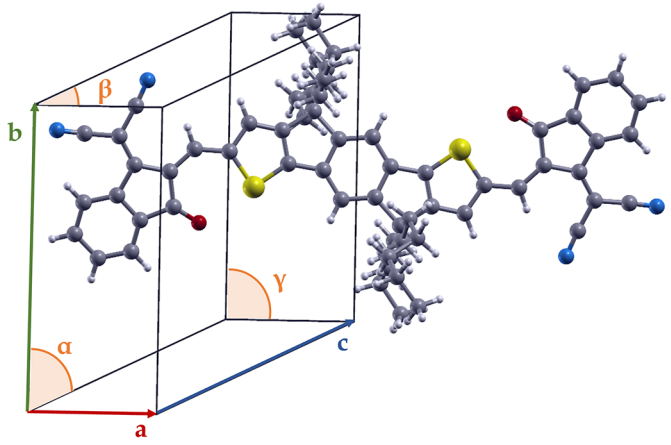

Fig. 6. Unit cell of the parent compound, IDIC-4H. Cell vectors and angles are also displayed.

Table 3. Unit cell lengths (a, b, c) in Å and angles (α, β, γ) in degrees for crystalline IDIC used in this work.

a	b	c	α	β	γ
8.6679	12.5073	13.5784	72.096	75.545	88.839

Table 4. Dihedral angles (θ) between IDT-IC planes and distances between the neighboring IDT planes.

	θ (degrees)	d_A (Å)	d_B (Å)
IDIC-4H	7.2	2.67	4.50
IDIC-4F	6.6	2.50	4.72
IDIC-4Cl	7.9	2.03	5.33

3.2 Crystal structure

To understand the relation between solid-state ordering and charge transfer, we thoroughly investigated three different systems, one for the halogen-free and two more for the halogenated IDIC molecules. The crystal structure of the parent compound IDIC-4H belongs to the centrosymmetric space group $P\bar{1}$ [59,60] and was taken from Cambridge Structural Database [61]. A schematic of the unit cell is given in Figure 6 while unit cell lengths and angles are listed in Table 3. Starting from the experimental structure, a geometry optimization was performed imposing periodic boundary conditions, while the unit cell vectors were kept fixed. Since experimentally resolved structures for IDIC-4F and IDIC-4Cl do not exist as of yet, the IC end group in pristine IDIC-4H was substituted by its fluorinated and chlorinated analogue as depicted in Figure 1. The resulting configurations were fully relaxed keeping however the unit cell vectors fixed.

In contrast to the gas phase, torsions are observed between the IDT core and the IC end groups, both for halogenated and pristine systems. Starting from the parent compound, the dihedral angle is calculated at 7.2°. After substituting fluorine atoms to the end groups, the dihedral angle acquired the smallest value (6.6°) while the substitution of chlorine atoms led to the most distorted configuration with a 7.9° dihedral angle (Tab. 4). The small distance between sulfur and oxygen (2.5 Å for IDIC-4Cl and 2.6 Å for IDIC-4H and IDIC-4F) can lead to noncovalent intermolecular interactions increasing planarity and rigidity of the three molecules. These interactions are defined as noncovalent conformational locks [62] and have been employed to boost the performance of π-conjugated polymers as well as small molecules.

A representative neighboring system is depicted in Figure 7 where hydrogen atoms are omitted for clarity. All three variants IDIC-4X (X=H,F,Cl) pack in a parallel-plane, face-to-face configuration. A nearest neighbor list is constructed by implementing a distance cutoff of 6 Å as described in Section 2.5. Four nearest neighbors correspond to each molecule and can be classified in two main categories based on the overlapping area. In Figure 7, R denotes the reference molecule, while M_n, $n = 1,...,4$ denote the four nearest neighbors. Since IDT cores are almost planar, in order to quantify neighbor proximity we measure the distance between IDT planes, denoted by d_A, d_B in Figure 7. Closest neighbors correspond to those with a large overlapping area while the most distant neighbors correspond to those where only the IC end groups overlap. Halogenation affects the neighbors' proximity by reducing the distance of closest molecules (M_2,M_3) and moving away the distant ones (M_1,M_4). Chlorinated IDIC is affected the most, compared to the fluorinated and halogen-free compound; closest neighbors are moved from 2.67 Å to 2.03 Å while the distant ones from 4.50 Å to 5.33 Å. The results are gathered in Table 4.

Electronic transfer integrals were calculated for all the non-equivalent nearest neighbors for the three crystal systems and are presented in Table 5. Results can be grouped based on two different criteria. The first one is

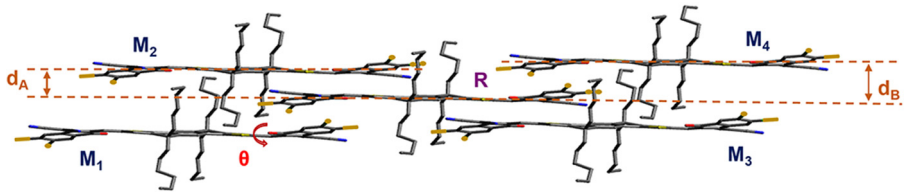

Fig. 7. Representative neighboring system for IDIC-4X, (X=H,F,Cl) with a reference molecule (R) and four nearest neighbors (M_1, M_2,M_3,M_4). Distance definitions for close (d_A) and distant (d_B) neighbors along with dihedral angle θ between the IDT core and IC end group are also displayed.

Table 5. Calculated transfer integral values for the four nearest neighbors (meV).

	M_1R	M_2R	M_3R	M_4R	Average
IDIC-4H	26	29	29	26	27.5
IDIC-4F	29	35	35	29	32.0
IDIC-4Cl	30	39	39	30	34.5

related to the closeness of the neighbors. The closest neighbors i.e., those with the largest overlapping area (M_2R, M_3R), give rise to the largest transfer integral values, both for the halogenated and halogen-free compounds, with the transfer integral of IDIC-4Cl reaching almost 40 meV. The most distant neighbors (M_1R, M_4R) give rise to the smaller values, ranging between 26 meV for IDIC-4H and 30 meV for IDIC-4Cl. At this point, we note that for a typical fullerene-based acceptor such as $PC_{61}BM$, a transfer integral value of 10 meV is reported [63], while in case of NFAs, Y5 exhibits an electronic coupling of 63.3 meV [13]. In addition, its π-extended counterpart yields 36.5 meV, whereas the fluorinated π-extended variant reaches a value of 103.8 meV [13]. The second classification is related to the effect of halogenation. The two halogenated conformations systematically present strengthened electronic coupling compared to the parent compound, both for the closest and the distant neighbors. In case of distant neighbors, the increase in transfer integral values is significant, even though halogenation moved them away. Specifically, it reaches 15.4% for IDIC-4Cl and 11.5% for IDIC-4F, with respect to the parent compound. In case where only the closest neighbors are considered, IDIC-4Cl exhibits an increase up to 34.5% and IDIC-4F up to 20.7%. Chlorinated IDIC exhibits the largest average electronic coupling, increased by 25.5% compared to the halogen-free IDIC and by 7.8% compared to fluorinated IDIC. Moreover, the average value of electronic coupling for fluorinated IDIC shows a 16.4% increase compared to IDIC-4H. Results are accumulated in Table 5.

Finally, Marcus rates for electron transport are calculated as described in Section 2.3. For the transfer integral we used the average value from Table 5 for each one of the halogen-free and the halogenated compounds while the temperature was set to 300 K. Rates are depicted in Figure 8, as a function of site energy difference (ΔG_{ij}) for the three molecules. Near the area of fast hopping rates, the parent compound, IDIC-4H, shows the lowest values

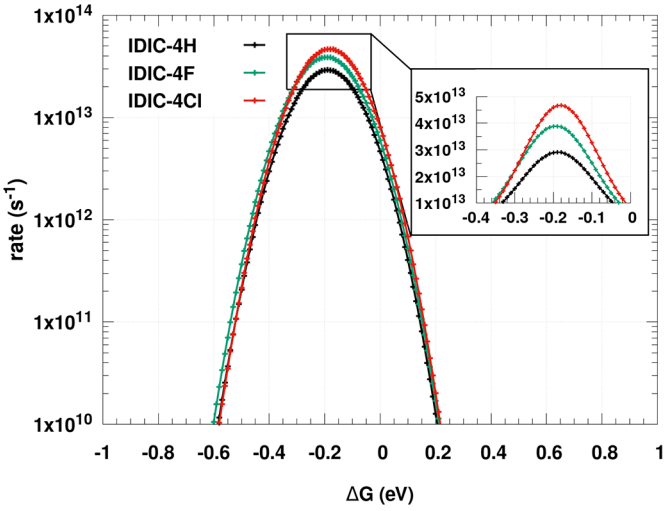

Fig. 8. Calculated Marcus rates as a function of site energy difference for the three variants.

compared to the halogenated molecules, whereas the highest values align with the chlorinated compound. The maximum value of transfer rate for IDIC-4Cl ($4.6 \times 10^{13}\,s^{-1}$) is boosted over 60% compared to the pristine configuration ($2.9 \times 10^{13}\,s^{-1}$). The fluorinated molecule, despite the largest value of reorganization energy develops rates ($3.9 \times 10^{13}\,s^{-1}$) faster up to 34% than IDIC-4H.

4 Conclusions

The non-fullerene acceptor, IDIC, was chosen as a model system so that the effects of end-group fluorination and chlorination could be systematically investigated. Using density functional theory, we examined the electronic and

optical properties of the isolated IDIC-4H, IDIC-4F and IDIC-4Cl molecules. Introducing halogens at the IC end group, deepens HOMO and LUMO energies and narrows the band gap, showing that halogenation leads to an improved electron accepting ability. Nonetheless, the distributions of the frontier molecular orbitals are not affected that much. The chlorinated compound shows the smallest value of reorganization energy and the largest values of EA and IP both adiabatic and vertical. Regarding the absorption spectrum, halogenated molecules exhibit redshift. In particular, chlorinated IDIC has the largest maximum absorption coefficient and the largest redshift (14 nm), whereas for fluorinated IDIC redshift is only 5 nm. Additionally, from the analysis of DOS arises that the major contribution to LUMO comes from the IC end groups, endorsing the idea that the terminal units are the key to charge transfer.

Lastly, based on the experimental crystal structure of IDIC-4H three crystal systems were constructed, one for each compound. The investigation of the transport systems revealed that nearest neighbors are categorized in two groups, depending on the overlapping area. Those with the larger overlapping area exhibit larger values of transfer integrals regardless the halogenation of the terminal units. However, halogenation increases the electronic coupling both for closest and distant neighbors. Once more, chlorinated IDIC shows the highest values of transfer integral, enhanced up to 25% compared to the plain IDIC while IDIC-4F shows a 16% increase. Calculation of transfer rates as a function of site energy difference, revealed an increase up to 60% for chlorinated IDIC and up to almost 34% for fluorinated IDIC despite the largest reorganization value. Our results confirm that halogenation of the IC edge units of NFAs, especially chlorination, can lead to a noteworthy change in the charge transport properties. In conclusion, end group modification with even larger halogens (Br or I) would be worth further investigation.

Acknowledgements. This work was supported by the European Union (European Social Fund) and Greece through the Operational Programme «Human Resources Development, Education and Lifelong Learning 2014–2020» (MIS 5047647).

Author contribution statement

MA and DGP conceived the idea. MA performed the calculations, analyzed the results and wrote the manuscript. KK and EL contributed in the analysis and visualization of the results. DGP acquired funding and supervised the research. All authors provided feedback and corrections to the manuscript.

References

1. O. Inganäs, Adv. Mater. **30**, 1800388 (2018)
2. L. Lu, T. Zheng, Q. Wu, A. Schneider, D. Zhao, L. Yu, Chem. Rev. **115**, 12666 (2015)
3. P.R. Berger, M. Kim, J. Renew. Sustain. Energy **10**, 013508 (2018)
4. H. Zhou, Y. Zhang, J. Seifter, S. Collins, C. Luo, G. Bazan, T.Q. Nguyen, A. Heeger, Adv. Mater. **25**, 1646 (2013)
5. Y. Liu, J. Zhao, Z. Li, W. Ma, H. Huawei, K. Jiang, H. Lin, H. Ade, He Yan, Nat. Commun. **5**, 5293 (2014)
6. J. Zhao, Y. Li, Y. Guofang, K. Jiang, H. Lin, H. Ade, W. Ma, He Yan, Nat. Energy **1**, 15027 (2016)
7. M. Zhang, L. Zhu, G. Zhou et al., Nat. Commun. **12**, 309 (2021)
8. Y. Cui, H. Yao, J. Zhang, T. Zhang, Y. Wang, L. Hong, K. Xian, B. Xu, S. Zhang, J. Peng, Z. Wei, F. Gao, J. Hou, Nat. Commun. **10**, 2515 (2019)
9. J. Huang, H. Tang, C. Yan, G. Li, Cell Rep. Phys. Sci. **2**, 100292 (2021)
10. Y. Lin, J. Wang, Z.G. Zhang, H. Bai, Y. Li, D.B. Zhu, X. Zhan, Adv. Mater. **27**, 1170 (2015)
11. Y. Lin, Q. He, F. Zhao, L. Huo, J. Mai, X. Lu, C.J. Su, T. Li, J. Wang, J. Zhu, Y. Sun, C. Wang, X. Zhan, J. Am. Chem. Soc. **138**, 2973 (2016)
12. J. Yuan, Y. Zhang, L. Zhou, C. Zhang, Lau Tsz. Ki, G. Zhang, X. Lu, H.L. Yip, Shu. So, Shu, S. Beaupre, M. Mainville, P. Johnson, M. Leclerc, H. Chen, H. Peng, Y. Li, Y. Zou, Adv. Mater. **31**, 1807577 (2019)
13. G. Li, X. Zhang, L.O. Jones, J. Alzola, S. Mukherjee, L.W. Feng, W. Zhu, C. Stern, J. Yu, V. Sangwan, D. DeLongchamp, K. Kohlstedt, M. Wasielewski, M. Hersam, G. Schatz, A. Facchetti, T. Marks, J. Am. Chem. Soc. **143**, 6123 (2021)
14. S.M. Swick, W. Zhu, M. Matta, T. Aldrich, A. Harbuzaru, J. Navarrete, O.R. Ponce, K. Kohlstedt, G. Schatz, A. Facchetti, F. Melkonyan, T. Marks, Proc. Natl. Acad. Sci. U. S. A. **115**, E8341 (2018)
15. C. Yao, C. Peng, Y. Yang, L. Li, M. Bo, J. Wang, J. Mater. Chem. C **6**, 4912 (2018)
16. F. Zhao, S. Dai, S. Wu, Y. Zhang, Q. Wang, J. Jiang, L. Ling, Q. Wei, Z. Ma, W. You, W. Wang, C. Zhan, X. Zhan, Adv. Mater. **29**, 1700144 (2017)
17. W. Zhao, S. Li, H. Yao, S. Zhang, Y. Zhang, B. Yang, J. Hou, J. Am. Chem. Soc. **139**, 7148 (2017)
18. T. Aldrich, M. Matta, W. Zhu, S. Swick, C. Stern, G. Schatz, A. Facchetti, F. Melkonyan, T. Marks, J. Am. Chem. Soc. **141**, 3274 (2019)
19. L. Shimoni, J.P. Glusker, Struct. Chem. **5**, 383 (1994)
20. Y. Wang, S. Parkin, J. Gierschner, M. Watson, Org. Lett. **10**, 3307 (2008)
21. J. Qu, H. Chen, J. Zhou, H. Lai, T. Liu, P. Chao, D. Li, Z. Xie, F. He, Y. Ma, ACS Appl. Mater. Interfaces **10**, 39992 (2018)
22. M. Tang, J. Oh, A. Reichardt, Z. Bao, J. Am. Chem. Soc. **131**, 3733 (2009)
23. A. Hiszpanski, J. Saathoff, L. Shaw, He. Wang, L. Kraya, F. Lüttich, M. Brady, M. Chabinyc, A. Kahn, P. Clancy, Y.L. Loo, Chem. Mater. **27**, 1892 (2015)
24. J. Yang, Q.S. Li, Z.S. Li, Phys. Chem. Chem. Phys. **23**, 12321 (2021)
25. J. Yang, Q.S. Li, Z.S. Li, Nanoscale **12**, 17795 (2020)
26. C. Yao, Y. Yang, L. Li, M. Bo, J. Zhang, C. Peng, Z. Huang, J. Wang, J. Phys. Chem. C **124**, 23059 (2020)
27. Y. Yang, Y. Chuang, L. Li, M. Bo, J. Jianfeng, C. Peng, Z. Huang, J. Wang, Dyes and Pigments **181**, 108542 (2020)

28. Y. Chuang, Y. Yang, L. Li, M. Bo, C. Peng, J. Wang, J. Mater. Chem. A **7**, 18150 (2019)
29. G. Forti, A. Nitti, P. Osw, R. Po, D. Pasini, Int. J. Mol. Sci. **21**, 8085 (2020)
30. Y. Lin, F. Zhao, S. Prasad, J. Chen, W. Cai, Q. Zhang, K. Chen, Y. Wu, W. Ma, F. Gao, J.X. Tang, C. Wang, W. You, J. Hodgkiss, X. Zhan, Adv. Mater. **30**, 1706363 (2018)
31. Y. Wu, Y. Zheng, H. Yang, C. Sun, Y. Dong, C. Cui, He. Yan, Y. Li, Sci. China Chem. **63**, 265 (2020)
32. Y. Zhang, G. Li, Acc. Mater. Res. **1**, 158 (2020)
33. M. Zhang, J. Zhu, K. Liu, G. Zheng, G. Zhao, L. Li, Y. Meng, T. Guo, H. Zhou, X. Zhan, J. Mater. Chem. A **5**, 24820 (2017)
34. A.D. Becke, Phys. Rev. A **38**, 3098 (1988)
35. C. Lee, W. Yang, R.G. Parr, Phys. Rev. B **37**, 785 (1988)
36. J. Wildman, P. Repiščák, M.J. Paterson, I. Galbraith, J. Chem. Theory Comput. **12**, 3813 (2018)
37. G. Raos, A. Famulari, V. Marcon, Chem. Phys. Lett., **379**, 364 (2003)
38. A. Tripathi, P. Chetti, Mol. Simul. **46**, 548 (2020)
39. J.P. Perdew, K. Burke, M. Ernzerhof, Phys. Rev. Lett. **77**, 3865 (1996)
40. J.P. Perdew, K. Burke, M. Ernzerhof, Phys. Rev. Lett. **78**, 1396 (1997)
41. D. Vanderbilt Phys. Rev. B **41**, 7892 (1990)
42. M.J. Frisch, G.W. Trucks, H.B. Schlegel, G.E. Scuseria, M.A. Robb, J.R. Cheeseman, J.A. Montgomery, Jr T. Vreven, K.N. Kudin, J.C. Burant, J.M. Millam, S.S. Iyengar, J. Tomasi, V. Barone, B. Mennucci, M. Cossi, G. Scalmani, N. Rega, G.A. Petersson, H. Nakatsuji, M. Hada, M. Ehara, K. Toyota, R. Fukuda, J. Hasegawa, M. Ishida, T. Nakajima, Y. Honda, O. Kitao, H. Nakai, M. Klene, X. Li, J.E. Knox, H. P. Hratchian, J.B. Cross, V. Bakken, C. Adamo, J. Jaramillo, R. Gomperts, R.E. Stratmann, O. Yazyev, A.J. Austin, R. Cammi, C. Pomelli, J.W. Ochterski, P.Y. Ayala, K. Morokuma, G.A. Voth, P. Salvador, J.J. Dannenberg, V.G. Zakrzewski, S. Dapprich, A.D. Daniels, M.C. Strain, O. Farkas, D.K. Malick, A.D. Rabuck, K. Raghavachari, J.B. Foresman, J.V. Ortiz, Q. Cui, A.G. Baboul, S. Clifford, J. Cioslowski, B.B. Stefanov, G. Liu, A. Liashenko, P. Piskorz, I. Komaromi, R.L. Martin, D.J. Fox, T. Keith, M.A. Al-Laham, C.Y. Peng, A. Nanayakkara, M. Challacombe, P.M. W. Gill, B. Johnson, W. Chen, M.W. Wong, C. Gonzalez, J.A. Pople, Gaussian 03, Revision E.01, Gaussian, Inc, Wallingford CT (2004)
43. P. Giannozzi, S. Baroni, N. Bonini, M. Calandra, R. Car, C. Cavazzoni, D. Ceresoli, G.L. Chiarotti, M. Cococcioni, I. Dabo, A. Dal Corso, S. Fabris, G. Fratesi, S. de Gironcoli, R. Gebauer, U. Gerstmann, C. Gougoussis, A. Kokalj, M. Lazzeri, L. Martin-Samos, N. Marzari, F. Mauri, R. Mazzarello, S. Paolini, A. Pasquarello, L. Paulatto, C. Sbraccia, S. Scandolo, G. Sclauzero, A.P. Seitsonen, A. Smogunov, P. Umari, R.M. Wentzcovitch, J. Phys.: Condens.Matter. **21**, 395502 (2009)
44. P. Giannozzi, O. Andreussi, T. Brumme, O. Bunau, M. Buongiorno Nardelli, M. Calandra, R. Car, C. Cavazzoni, D. Ceresoli, M. Cococcioni, N. Colonna, I. Carnimeo, A. Dal Corso, S. de Gironcoli, P. Delugas, R.A. DiStasio, Jr A. Ferretti, A. Floris, G. Fratesi, G. Fugallo, R. Gebauer, U. Gerstmann, F. Giustino, T. Gorni, J. Jia, M. Kawamura, H.Y. Ko, A. Kokalj, E. Küçükbenli, M. Lazzeri, M. Marsili, N. Marzari, F. Mauri, N.L. Nguyen, H.V. Nguyen, A. Otero-de-la-Roza, L. Paulatto, S. Poncé, D. Rocca, R. Sabatini, B. Santra, M. Schlipf, A.P. Seitsonen, A. Smogunov, I. Timrov, T. Thonhauser, P. Umari, N. Vast, X. Wu, S. Baroni, J. Phys.: Condens. Matter **29**, 465901 (2017)
45. N.M. O'Boyle, A.L. Tenderholt, K.M. Langner, J. Comp. Chem. **29**, 839 (2008)
46. E. Aprà, E.J. Bylaska, W.A. de Jong, N. Govind, K. Kowalski, T.P. Straatsma, M. Valiev, H.J.J. van Dam, Y. Alexeev, J. Anchell, V. Anisimov, F.W. Aquino, R. Atta-Fynn, J. Autschbach, N.P. Bauman, J.C. Becca, D.E. Bernholdt, K. Bhaskaran-Nair, S. Bogatko, P. Borowski, J. Boschen, J. Brabec, A. Bruner, E. Cauët, Y. Chen, G.N. Chuev, C.J. Cramer, J. Daily, M.J.O. Deegan, T.H. Dunning, Jr, M. Dupuis, K.G. Dyall, G.I. Fann, S.A. Fischer, A. Fonari, H. Früchtl, L. Gagliardi, J. Garza, N. Gawande, S. Ghosh, K. Glaesemann, A.W. Götz, J. Hammond, V. Helms, E.D. Hermes, K. Hirao, S. Hirata, M. Jacquelin, L. Jensen, B.G. Johnson, H. Jónsson, R.A. Kendall, M. Klemm, R. Kobayashi, V. Konkov, S. Krishnamoorthy, M. Krishnan, Z. Lin, R.D. Lins, R.J. Littlefield, A.J. Logsdail, K. Lopata, W. Ma, A.V. Marenich, J. Martin del Campo, D. Mejia-Rodriguez, J.E. Moore, J.M. Mullin, T. Nakajima, D.R. Nascimento, J.A. Nichols, P.J. Nichols, J. Nieplocha, A. Otero-de-la-Roza, B. Palmer, A. Panyala, T. Pirojsirikul, B. Peng, R. Peverati, J. Pittner, L. Pollack, R.M. Richard, P. Sadayappan, G.C. Schatz, W.A. Shelton, D.W. Silverstein, D.M.A. Smith, T.A. Soares, D. Song, M. Swart, H.L. Taylor, G.S. Thomas, V. Tipparaju, D.G. Truhlar, K. Tsemekhman, T. Van Voorhis, Á. Vázquez-Mayagoitia, P. Verma, O. Villa, A. Vishnu, K.D. Vogiatzis, D. Wang, J.H. Weare, M.J. Williamson, T.L. Windus, K. Wolinski, A.T. Wong, Q. Wu, C. Yang, Q. Yu, M. Zacharias, Z. Zhang, Y. Zhao, R.J. Harrison, J. Chem. Phys. **152**, 184102 (2020)
47. G. Hutchison, M. Ratner, T. Marks, J. Am. Chem. Soc. **127**, 2339 (2005)
48. R.A. Marcus, Rev. Mod. Phys. **65**, 599 (1993)
49. Q. Wang, Y. Li, P. Song, R. Su, F. Ma, Y. Yang, Polymers **9**, 692 (2017)
50. G. Han, Y. Guo, L. Ning, Y. Yi, Sol. RRL **3**, 1800251 (2019)
51. J.L. Brédas, D. Beljonne, V. Coropceanu, J. Cornil, Chem. Rev. **104**, 4971 (2004)
52. J. Kirkpatrick, Int. J. Quantum Chem. **108**, 51 (2008)
53. B. Baumeier, J. Kirkpatrick, D. Andrienko, Phys. Chem. Chem. Phys. **12**, 11103 (2010)
54. E. Valeev, V. Coropceanu, D. Da Silva Filho, S. Salman, J.L. Brédas, J. Am. Chem. Soc. **128**, 9882 (2006)
55. P.O. Löwdin, J. Chem. Phys. **18**, 365 (1950)
56. A. Pal, L.K. Wen, C.Y. Jun, I. Jeon, Y. Matsuo, S. Manzhos, Phys. Chem. Chem. Phys. **19**, 28330 (2017)
57. N.R. Tummala, Z. Zheng, S.G. Aziz, V. Coropceanu, J.-L. Brédas, J. Phys. Chem. Lett. **6**, 3657 (2015)
58. N.R. Tummala, S.A. Elroby, S.G. Aziz, C. Risko, V. Coropceanu, J.-L. Brédas, J. Phys. Chem. C **120**, 17242 (2016)
59. P. Mondelli, G. Boschetto, P.N. Horton, P. Tiwana, C.-K. Skylaris, S.J. Coles, M. Krompiec, G. Morse, Mater. Horiz. **7**, 1062 (2020)

60. P. Mondelli, G. Boschetto, P.N. Horton, P. Tiwana, C.-K. Skylaris, S.J. Coles, M. Krompiec, G. Morse, Deposition Number (CSD): 1942951, DOI: 10.5517/ccdc.csd.cc236svz
61. C.R. Groom, I.J. Bruno, M.P. Lightfoot, S.C. Ward, Acta Cryst. **B72**, 171 (2016)
62. H. Huang, L. Yang, A. Facchetti, T.J. Marks, Chem. Rev. **117**, 10291 (2017)
63. J.C. Aguirre, C. Arntsen, S. Hernandez, R. Huber, A.M. Nardes, M. Halim, D. Kilbride, Y. Rubin, S.H. Tolbert, N. Kopidakis, B.J. Schwartz, D. Neuhauser, Adv. Funct. Mater. **24**, 784 (2014)

Cite this article as: Maria Andrea, Konstantinos Kordos, Elefterios Lidorikis, Dimitrios Papageorgiou, Fluorination and chlorination effects on the charge transport properties of the IDIC non-fullerene acceptor: an ab-initio investigation, EPJ Photovoltaics **13**, 15 (2022)